Nonequilibrium phase transition in a self-activated biological network

Hugues Berry*

Equipe de Recherche sur les Relations Matrice Extracellulaire-Cellules (ERRMECe), Département de Biologie, Université de Cergy-Pontoise, Boîte Postale 222, 2 Avenue A. Chauvin, 95302 Cergy-Pontoise Cedex, France

(Received 2 October 2002; revised manuscript received 16 December 2002; published 14 March 2003)

We present a lattice model for a two-dimensional network of self-activated biological structures with a diffusive activating agent. The model retains basic and simple properties shared by biological systems at various observation scales, so that the structures can consist of individuals, tissues, cells, or enzymes. Upon activation, a structure emits a new mobile activator and remains in a transient refractory state before it can be activated again. Varying the activation probability, the system undergoes a nonequilibrium second-order phase transition from an active state, where activators are present, to an absorbing, activator-free state, where each structure remains in the deactivated state. We study the phase transition using Monte Carlo simulations and evaluate the critical exponents. As they do not seem to correspond to known values, the results suggest the possibility of a separate universality class.

DOI: 10.1103/PhysRevE.67.031907 PACS number(s): 87.10.+e, 87.16.Yc, 64.60.−i, 05.70.Ln

I. INTRODUCTION

Continuous nonequilibrium phase transitions have been studied in a number of biologically relevant models, including forest fire or epidemics spreading [1], biological evolution [2,3], population dynamics [4], or cell interactions in immune system [5]. Close to the transition, such critical systems are not very sensible to the detailed nature of the dynamical rules they rely on, but rather depend on more fundamental characteristics such as symmetries or Euclidean dimensions. As a result, a qualitative glance on complex auto-organized systems, such as biological ones, can be obtained by studying even simple models.

Self-organization in biological systems relies on functional interactions between populations of structural units, whether individuals, organs, tissues, cells, or molecules. Commonly, these interactions take the form of activating or infecting messages that act in a nonlocal and noninstantaneous way. For instance, cell growth is mainly controlled by extracellularly diffusing growth factors that act on the source cell that emitted it (autocrine signaling) or on a neighboring cell (paracrine signaling) [6]. Upon stimulation by growth factors, the quiescent target cell enters the $G1$-S cell-cycle phase [7], eventually leading to cell proliferation as well as synthesis (and excretion) of new growth factors, as a result of a positive feedback loop [8]. Strikingly, similar basic organization schemes are encountered at several observation scales. We illustrate here some shared basic design principles with the cases of allosteric-enzyme networks, cell population organization (such as *Dictyostelium discoideum*) or virus spreading through air dissemination. Although very dissimilar, these examples share common features.

(i) The infecting or activating messenger acts remotely, through diffusional (or nondirectional) transport. For instance, the catalytic constants of many allosteric enzymes from metabolic networks are controlled by the enzyme reaction-product diffusing inside the cell [9]. Similarly to the growth factors in the above-mentioned case of auto-paracrine control of cell growth, extracellular cyclic adenosine monophosphate (cAMP) diffuses between *Dictyostelium discoideum* cells upon starvation and regulates their behavior [10,11]. This is also the case of several infection spreading mechanisms where infected individuals can infect other distant individuals in the absence of body-to-body contact, via the emission of the infectious agent in the air. This infection mode has, for example, been evidenced for the foot-and-mouth disease [12] or the influenza virus (flu) transmission [13].

(ii) Upon encounter with the mobile messenger, the structure under consideration switches to an activated state. During this activated state, a positive feedback loop leads to the formation and excretion of new mobile messengers. In product-activated allosteric-enzyme networks, the diffusing product favors the initiation of the enzyme catalytic cycle, that ultimately leads to the formation of a new reaction product. Growth factor stimulation of eucaryotic cells, as well as cAMP stimulation of *D. discoideum*, triggers intracellular signalization cascades that increase the synthesis and excretion rates of these factors by the cell [14,16]. In the case of epidemic air dissemination, infected individuals (such as pigs in the foot-and-mouth disease [15]) often secrete vast amounts of infectious agent and become sources of its air dissemination.

(iii) Another feature often displayed by these biological systems is the existence of a refractory or lag phase: after activation by the messenger, a time lapse must be waited before the target structure can be activated again. This feature is intrinsic to enzyme conformational cycles, that must be completed before the enzyme finds itself in the (free) resting conformation. Such lag phases are also encountered in cell communication systems: once stimulated by growth factors, eucaryotic cells show a desensitized state because of growth-factor membrane receptor down regulation [17]. Furthermore, once initiated, the cell cycle enters a growth-factor independent phase that must be completed before the cell initiates a new cycle [7]. A similar lag phase is also observed in *D.* Discoideum cells after cAMP stimulation, during which these cells are refractory to cAMP [18]. In the case of

*Electronic address: hugues.berry@bio.u-cergy.fr

epidemic spreading, this delay or lag phase is intrinsic to the contamination process, since an infected individual must recover before being infected again.

Seen from this angle, these systems can be compared to self-organized critical models of sandpiles, avalanches, or earthquakes [19]. However, self-organized critical systems are slowly driven systems [20]. In the biological systems mentioned above, the time scale for messenger transport to the target structure is usually not shorter than the internal dynamics of the structure. They are thus not slowly driven and their dynamics must be separately addressed.

In the present paper, we study a very simple two-dimensional lattice model that displays these basic properties. Each activable structure is considered to be immobile with respect to the messenger which is assumed to move by diffusion on the lattice. Upon encounter of a messenger with an activable structure, the latter activates with probability ω. When activated, a structure emits a new messenger and remains in a refractory state before another messenger can activate it again. We use Monte Carlo simulations to investigate the behavior of this system in two dimensions, as the activation probability ω is varied. The paper is organized as follows. The following section describes the model, of which a mean-field study is presented in Sec. III. In Sec. IV, results of Monte Carlo simulations are shown and evidence absorbing-phase transition as ω is varied. Studies of the dynamical critical behavior as well as finite-size scaling analysis allow to estimate the critical exponents. Finally, Sec. V presents a short discussion concerning the universality class of the model.

II. THE MODEL

Our model is basically a two-dimensional version of the zero-dimensional model for allosteric enzyme networks of Mikhailov and Hess [21], without spontaneous activation. It consists of N activable biological units regularly distributed over a two-dimensional lattice of (linear) length L. Broadly speaking, these units can represent individuals, tissues, cells, or enzymes and will be designated in the following by the general term of *structures*. The distance l between two nearest-neighbor structures is constant, with $l=L/\sqrt{N}$. To model the activation as well as the refractory phase, we associate each structure $i=1,\ldots,N$ with a dynamical variable $\phi_i(t)$ that takes integer values between 0 and K and represents the structure state at time t (Fig. 1). The state $\phi_i=0$ is the activable state. The transition from $\phi_i=0$ to $\phi_i=1$ represents the activation of the structure and occurs with probability ω if an activating messenger A is present on the structure site. The transitions from the state $\phi_i=j$ to $\phi_i=j+1$ then occurs with rate 1, for $j=1,\ldots,K-1$. After K steps, the structure is back in the activable state, i.e., goes from $\phi_i=K-1$ to $\phi_i=0$ with rate 1. Thus, once activated, a given structure must wait $K-1$ time units to find itself back in the activable state. Finally, the conformation state $\phi_i=K_r$ ($1<K_r<K$) is the messenger-releasing step, i.e., the transition from $\phi_i=K_r-1$ to $\phi_i=K_r$ is accompanied by the release of an activating messenger A on the structure i site.

The structures are considered as immobile, whereas the A molecules are allowed to diffuse over the lattice (random walk). The A molecules are assumed to have a finite lifetime and are removed from the lattice with rate λ. For simplicity, in this study, we fix the values of λ, K, and K_r, so that the model only depends on the activation probability ω. In the following, the model behavior is studied as ω is varied.

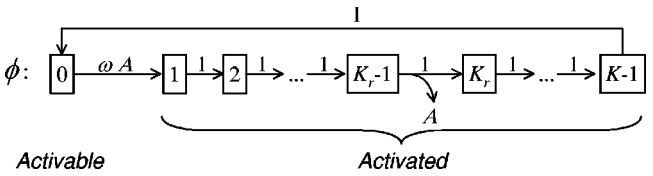

FIG. 1. Evolution of a structure state ϕ. The activable state is $\phi=0$. A structure can be activated to the first step of the activated state $\phi=1$ with probability ω if an activator A is present on the structure site. The structure then remains in the activated state during $K-1$ time steps (refractory phase) and releases a new mobile activator upon transition from state K_r-1 to the next one. After $K-1$ refractory steps, the structure is back in the activable state $\phi=0$.

III. MEAN-FIELD ANALYSIS

The model can be described by the following set of reactions:

$$A+S_0 \overset{\omega}{\rightarrow} A+S_1,$$

$$S_i \overset{1}{\rightarrow} S_{i+1}, \quad i=1,\ldots,K_r-2,K_r,\ldots,K-2,$$

$$S_{K_r-1} \overset{1}{\rightarrow} S_{K_r}+A,$$

$$S_{K-1} \overset{1}{\rightarrow} S_0,$$

$$A \overset{\lambda}{\rightarrow} \varnothing,$$

where S_i designates a structure S in the state $\phi=i$, A is the activating messenger, and superscripts on arrows designate reaction probabilities or rates. The classical mean-field (spatially homogeneous) equations for these reactions are readily found to be

$$d\sigma_0/dt=-\omega\rho\sigma_0+\frac{N}{L^2}-\sum_{i=0}^{K-2}\sigma_i, \tag{1a}$$

$$d\sigma_1/dt=\omega\rho\sigma_0-\sigma_1, \tag{1b}$$

$$d\sigma_i/dt=\sigma_{i-1}-\sigma_i, \quad i=2,\ldots,K-2, \tag{1c}$$

$$d\rho/dt=\sigma_{K_r-1}-\lambda\rho, \tag{1d}$$

where σ_i represents the density of structures in conformational state $\phi=i$ and ρ, the activator density. In Eq. (1a), conservation of the total structure density has been used: $\sigma_{K-1}=N/L^2-\Sigma_{i=0}^{K-2}\sigma_i$.

Equations (1) have two steady states:

$$\sigma_0=N/L^2, \tag{2a}$$

$$\sigma_i=0, \quad i=1,\ldots,K-1, \tag{2b}$$

$$\rho=0; \tag{2c}$$

and

$$\sigma_0=\lambda/\omega, \tag{3a}$$

$$\sigma_i=\frac{1}{K-1}\left(\frac{N}{L^2}-\frac{\lambda}{\omega}\right), \quad i=1,\ldots,K-1, \tag{3b}$$

$$\rho=\frac{1}{K-1}\left(\frac{N}{\lambda L^2}-\frac{1}{\omega}\right). \tag{3c}$$

The first steady state [Eqs. (2)] is an absorbing state: if the system reaches this configuration, it cannot escape from it. The second steady state [Eqs. (3)] will be referred to as the active state. Note that, in both cases, the steady states do not depend on the value of the activator-releasing state of the structures (K_r). The stability of these two steady states can be determined analytically for $K\leqslant 4$. The two steady states undergo a transcritical bifurcation at $\omega=\omega_c=\lambda L^2/N$, the active state being stable for $\omega>\omega_c$ and the absorbing one for $\omega<\omega_c$.

In the case of the fly *Drosophilia* oogenesis, it was found that growth factors excreted by a given cell can act over a spatial range of three to four intercell distances [22]. In the present model, the spatial range of the diffusing messenger is mainly dictated by its survival probability λ. Accordingly, the value of λ has been fixed so that the mean lifetime of a mobile messenger corresponds to the average time needed for it to walk over a distance corresponding to three interstructure distance l i.e., $\lambda=1/(3l)^2$. Because we use $l=7$ in the present study, $\lambda=1/441$, and mean-field analysis predicts an absorbing-state phase transition at $\omega_c=1/9$. For $K>4$, the stability can be studied numerically. As can be seen from Fig. 2, the behavior of the system is qualitatively conserved. The stability of the steady states does not depend on K, and the absorbing-phase transition is maintained at $\omega_c=1/9\approx 0.1111$. In the active phase, the activator density

$$\rho=\frac{1}{K-1}\left(\frac{1}{\omega_c}-\frac{1}{\omega}\right)\sim\omega-\omega_c, \tag{4}$$

which defines the critical exponent β in the mean-field approximation, $\beta_{MF}=1$.

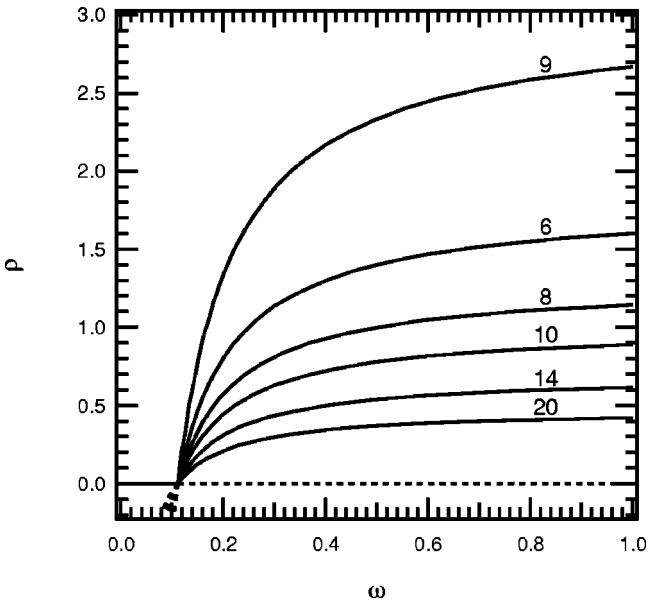

FIG. 2. Numerical study of the steady-state stability for the mean-field approximation as a function of the activation probability ω. A transcritical bifurcation is observed for all K at $\omega=\omega_c\approx 0.1111$. Full lines represent stable steady states and dotted lines unstable ones. The numbers above the curves indicate the corresponding value of K. For each curve $K_r=1+(K/2)$, $l=7$, $N=100$, and $\lambda=1/441$. Note that the absorbing steady state $\rho=0$ does not depend on ω. This continuation study was realized numerically using the program AUTO [23].

IV. MONTE CARLO SIMULATIONS AND RESULTS

A. Description

The model is studied by Monte Carlo simulations on two-dimensional square lattices with periodic boundaries. Multiple occupancy of a site is allowed, so that a lattice site can be occupied by several activators at a given time (bosonic model). The distance between two nearest-neighbor structures is exactly l lattice sites. The implementation of the above dynamic rules on a computer is straightforward. At each Monte Carlo step, the system is updated as follows. The structure conformation variables ϕ_i, with $i=1,\ldots,N$ are updated simultaneously for each structure i, in agreement with Fig. 1. Note that, as multiple occupancy of a site is allowed for an activator molecule, the presence of n activators on structure site i increases the transition probability: $P(\phi_i=0\rightarrow\phi_i=1)=1-(1-\omega)^n$. The positions of the activator molecules are then updated: new activators are created at each structure site for which the conformation variable $\phi_i=K_r$ and each activator is removed from the lattice with probability λ. Finally, the surviving activators are independently and simultaneously moved to randomly chosen nearest-neighbor sites (Von Neumann neighborhood). The various probabilities are simulated using uniformly distributed random numbers generated with the combined generator of Ref. [24].

B. Dynamical behavior

Figure 3 shows ρ and σ_0 time evolutions for $L=70$ and $l=7$. For low activation probabilities (see $\omega=0.12$ in Fig.

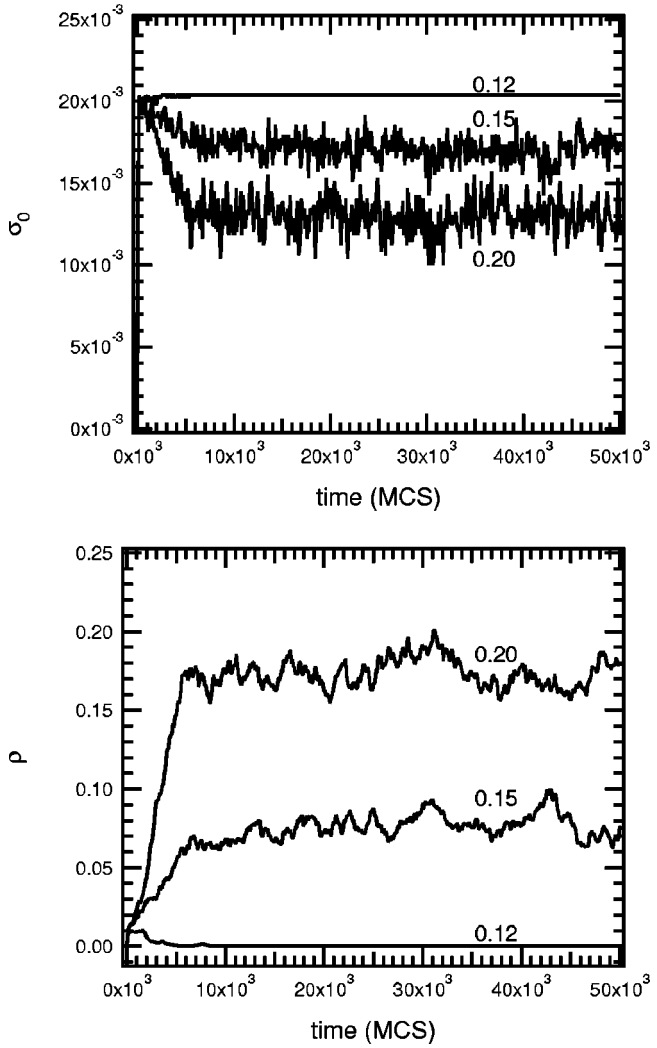

FIG. 3. Time evolution of the density of structures in the activable state (σ_0, top) and of the activator density (ρ, bottom) during a single Monte Carlo simulation initiated without activator and with random structure states ϕ. The numbers on the curves are the values of the probability ω. Time is expressed as Monte Carlo steps (MCS). Parameters are: $L=70$, $K=20$, $K_r=11$, $l=7$, $\lambda=1/441$, and $N=100$. The total structure density is thus 0.0204.

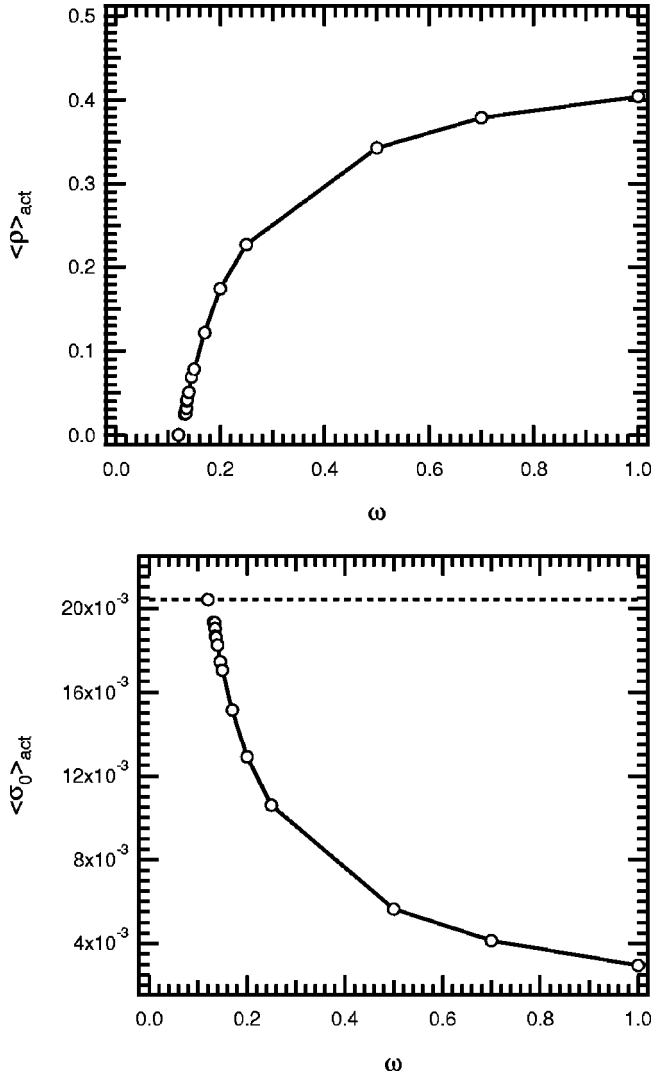

FIG. 4. Dependance on probability ω of the average densities of activating molecules (top) and activable structures (bottom), in the active state. The dotted line indicates the total structure density. The full lines are guides for the eyes. Other simulation parameters are as in Fig. 3.

3), the system rapidly tends to the absorbing steady state [Eqs. (2)]. With higher probabilities, the densities reach at longer times a fluctuating active state, with average values depending on the probability ω.

Figure 4 shows the dependance of the average densities in the active steady state $\langle\sigma_0\rangle_{act}$ and $\langle\rho\rangle_{act}$, as a function of ω. These simulations clearly confirm the occurrence of a second-order (continuous) phase transition from the active state to the absorbing state. The threshold ω_c is seen from Fig. 4 to be close to 0.13, slightly higher than the value obtained from the mean-field approximation.

To determine more precisely the critical probability and evaluate the critical exponents, we first present Monte Carlo simulations initiated with a lattice containing one activator molecule per lattice site and random structure states. In the case of a continuous phase transition, the activator density $\rho(t)$ is expected to scale as [25]

$$\rho(t)\sim t^{-\alpha} f(\Delta t^{1/\nu_\parallel}), \tag{5}$$

where f is a universal scaling function, $\Delta=|\omega-\omega_c|$ is the distance from the threshold, and $\nu_\parallel$ is the correlation length exponent (in the time direction). According to Eq. (5), $\rho(t)$ decreases as a power law at criticality

$$\rho(t)\sim t^{-\alpha}, \qquad \omega=\omega_c. \tag{6}$$

Figure 5 shows a plot of $\rho(t)$ for various values of ω. At criticality, one expects these curves to form straight lines, whereas off-critical values should show curvatures at long times. Simulations with $\omega\geqslant 0.130$ are clearly above the threshold, while those with $\omega\leqslant 0.124$ are subcritical. In order to obtain more precise estimations, the local slopes of these curves are also shown in the top right panel. Average local slopes are calculated as [26,27]

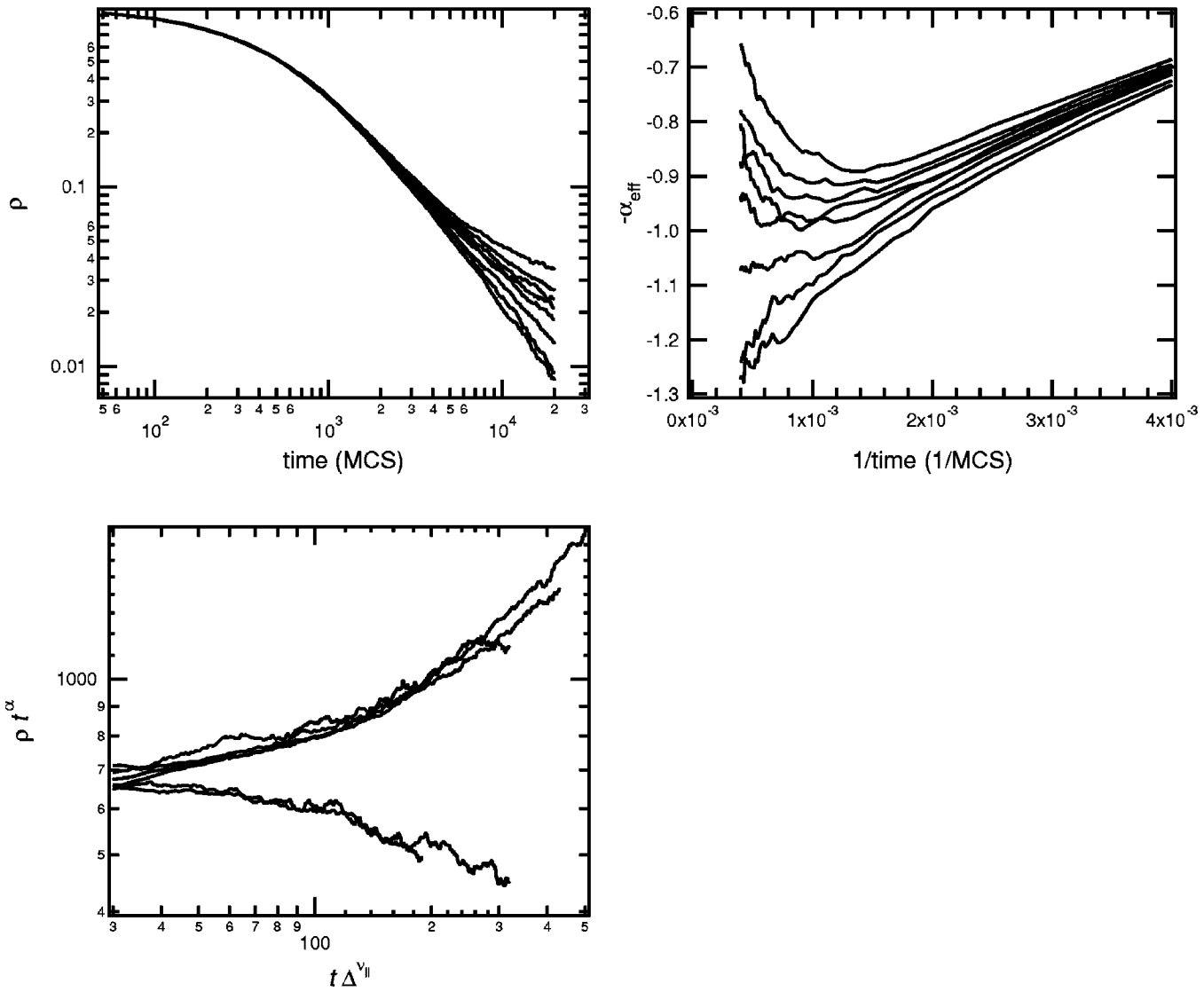

FIG. 5. Results of Monte Carlo simulations initiated with one activator per lattice site and random structure states ϕ (top left). Time evolution of the activator density ρ. Probabilities are (from bottom to top) $\omega=0.122$, 0.124, 0.126, 0.128, 0.129, 0.130, 0.132, 0.134. Results are averages of 100 (for $\omega=0.126$) or 50 (for the other probabilities) independent runs (top right). Plots of the corresponding local slope $-\alpha(t)$. Probabilities are as in left panel (bottom). Scaling of $\rho(t)$ as ρt^{α} versus $t\times\Delta^{\nu_\parallel}$ with $\omega_c=0.127$, $\alpha=1.1$, and $\nu_\parallel=0.75$. Other simulation parameters are as in Fig. 3.

$$-\alpha(t)=\frac{\log_{10}[\rho(t)/\rho(t/m)]}{\log_{10} m}. \tag{7}$$

The value $m=8$ is used here. Generally, one expects corrections to the power law Eq. (6) of the type

$$\rho(t)\sim t^{-\alpha}\left(1+\frac{a}{t}+\frac{b}{t^{\alpha'}}+\cdots\right). \tag{8}$$

The local slope thus behaves according to

$$\alpha(t)=\alpha+\frac{a}{t}+\frac{\alpha' b}{t^{\alpha'}}+\cdots. \tag{9}$$

Hence, in a plot of the local slopes versus $1/t$, the critical exponent is the intercept of the curve for $\omega=\omega_c$ with the y axis, and the curves for off-critical values are expected to show notable curvatures. Inspection of the corresponding curve in Fig. 5 shows that $0.126\leqslant\omega_c\leqslant0.128$. Furthermore, we evaluate from this figure $\alpha=1.1(1)$, where the uncertainty in the last digit is shown in parentheses.

According to Eq. (5), plots of ρt^{α} versus $t\Delta^{\nu_\parallel}$ should collapse on a single curve with upward curvature for $\omega>\omega_c$ and another one with downward curvature for $\omega<\omega_c$ [25]. The best collapse for the data of Fig. 5 is obtained with $\nu_\parallel=0.75$ (Fig. 5, bottom panel). With these estimations, another critical exponent can be evaluated: $\beta=\alpha\nu_\parallel\approx0.82$. β is the critical exponent relating the activator density in the active state to the distance from the threshold

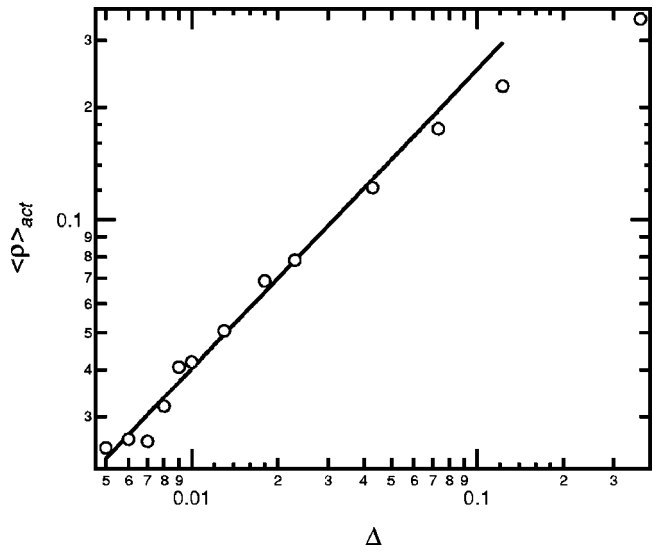

FIG. 6. Plot of the data of Fig. 4 for probabilities close to the threshold as a function of the distance $\Delta=|\omega-\omega_c|$, for $\omega_c=0.127$. The full line has a slope of 0.80.

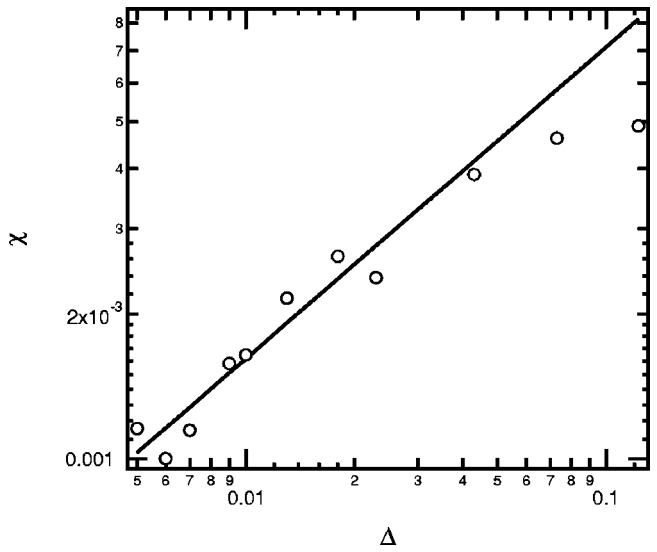

FIG. 7. Steady-state fluctuations of the density of structures in the activable state σ_0 as a function of the distance to the threshold $\Delta=|\omega-\omega_c|$, for $\omega_c=0.127$. The full line has a slope of 0.64. Other simulation parameters are as in Fig. 3.

$$\langle\rho\rangle_{act}\sim\Delta^{\beta}. \tag{10}$$

As a consistency check, Fig. 6 shows the data of Fig. 4 for ω close to the threshold as a function of Δ, in log-log coordinates. From the slope of the data, we estimate $\beta=0.80$, in good agreement with the value deduced from α and $\nu_{\|}$. This value is significantly lower than predicted by the mean-field approximation ($\beta_{MF}=1$).

It can be observed from Fig. 3 that fluctuations around the average steady-state values are higher for $\omega=0.20$ than for $\omega=0.15$. This is particularly obvious for σ_0. The density fluctuations in the active state $\chi=L^2(\langle\sigma_0^2\rangle-\langle\sigma_0\rangle^2)$ are expected to scale close to the critical point as

$$\chi\sim\Delta^{-\gamma}. \tag{11}$$

In the model studied here, fluctuations around the steady-state value in the active state increase as the distance to the threshold increases, implying a negative value for γ. Figure 7 shows that χ increase satisfies Eq. (11), with $\gamma=-0.64$. Note that a similar value (-0.66) is obtained with ρ fluctuations, albeit with poorer statistics.

To obtain other exponents, so-called "dynamic" Monte Carlo simulations [26–28] have also been performed. They consist in initiating the simulations with a configuration very close to the absorbing state, and measuring the time evolution of the number of activating molecules present at time t, $N(t)$, and the probability that the system has not entered the absorbing state at this time, $P(t)$, averaged over many realizations. These quantities scale at criticality in the long-time limit as [26,27]

$$N(t)\sim t^{\eta},\quad P(t)\sim t^{-\delta},\quad \omega=\omega_c. \tag{12}$$

The main advantage of these simulations is their absence of dependence on the system size [25]. Dynamic Monte Carlo simulations were initiated with a unique product molecule at a random position, and all structures in the activable state $\phi=0$. The surviving probability and the number of product molecules were recorded during 2×10^4 Monte Carlo steps, and averaged over 2×10^3 realizations.

Figure 8 shows the results of these simulations for $N(t)$ and $P(t)$. The local slopes are evaluated as already described for α. From the results for effective exponent η (Fig. 8, left panel), we estimate $\omega_c\approx0.128$, whereas its value from effective exponent δ (Fig. 8, right panel) is lower: $\omega_c\approx0.126$. Thus, the critical probability can be evaluated from these results to $\omega_c=0.127(1)$. The two critical exponents can be estimated from the long-time behavior of the local slopes to $\eta=0.18(5)$ and $\delta=0.82(8)$. Finally, another critical exponent can be estimated from these values: $\beta'=\delta\nu_{\|}\approx0.62$.

C. Finite-size scaling

Because of the finite size of the lattice in the simulations, the activator density is expected to depend on the lattice size L at criticality as [25]

$$\rho(L,t)\sim t^{-\alpha}g(t^{1/z}/L),\quad \omega=\omega_c, \tag{13}$$

where g is a universal scaling function, $z=\nu_{\|}/\nu_{\perp}$ is the dynamic exponent, and $\nu_{\perp}$ is the correlation length exponent in the space direction. To determine the dynamic exponent, Monte Carlo simulations were carried out at criticality with variable lattice sizes L, but keeping the interstructure length l constant (Fig. 9). As predicted by Eq. (13), the data for various L plotted as ρt^{α} versus t/L^z should collapse on the same curve. The inset in Fig. 9 show the best collapse of these data, obtained for $z=1.62$.

As a consistency check, the characteristic time of the system, τ, was also estimated during these simulations. As a

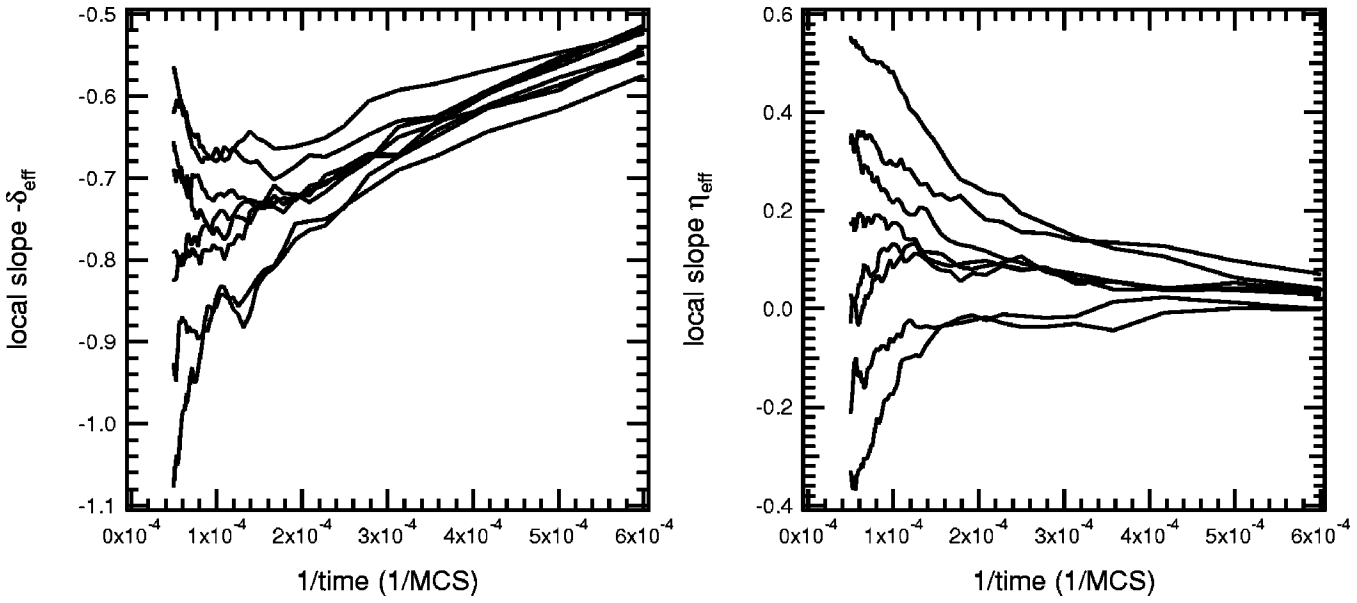

FIG. 8. Local slopes (effective exponents) for the number of activating molecules $N(t)$ (left) and the survival probability $P(t)$ (right) in dynamic Monte Carlo simulations. Probabilities are (from bottom to top) $\omega=0.122$, 0.124, 0.126, 0.127, 0.128, 0.129, 0.130, 0.132. Results are averages of 2×10^3 independent runs for each probability. Other simulation parameters are as in Fig. 3.

characteristic time, the time for the system to reach the absorbing state was chosen. At criticality, τ is expected to scale for finite systems as

$$\tau(L)\sim L^z, \qquad \omega=\omega_c . \tag{14}$$

Following Ref. [30], we evaluate for each sample the moment

$$\tau_s(L)=\sum_t t\rho(t) \Big/ \sum_t \rho(t), \tag{15}$$

$\tau(L)$ is the ensemble average over 50 samples at a given lattice size, $\tau(L)=\langle\tau_s\rangle$. Figure 10 shows a plot of $\tau(L)$ as a function of L, indicating the value of $z=1.59$, in good agreement with the previously estimated value. Finally, the value of $\nu_\perp$ can be estimated from z and $\nu_\parallel$ to $\nu_\perp=\nu_\parallel/z=0.47$.

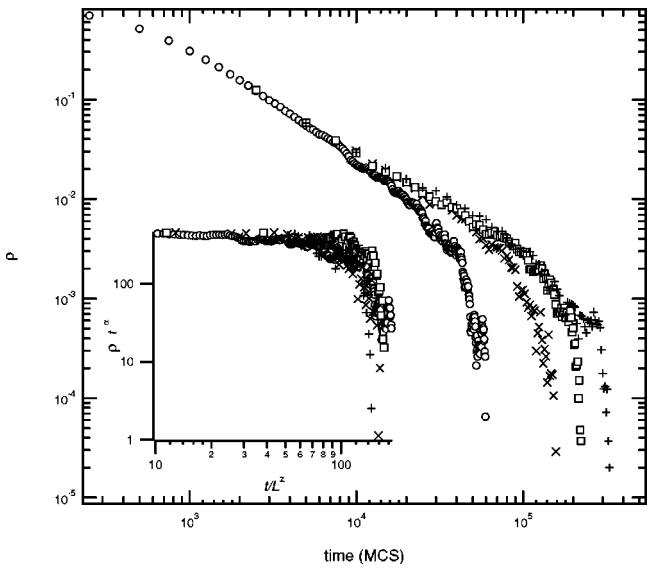

FIG. 9. $\rho(L,t)$ versus time at criticality, for various lattice sizes, $L=35$ (○), 70 (×), 84 (□), or 119 (+). Simulations initiated with one activator per lattice site and random structure states. Shown are averages of 50 independent runs for each size. $\omega=0.127$, $l=7$, and other simulation parameters as in Fig. 3. *Inset*: Scaling of $\rho(L,t)$ as ρt^α versus t/L^z, with $\alpha=1.10$ and $z=1.62$.

V. DISCUSSION

We have presented Monte Carlo simulations for a lattice model of self-activation in a network of biological structures

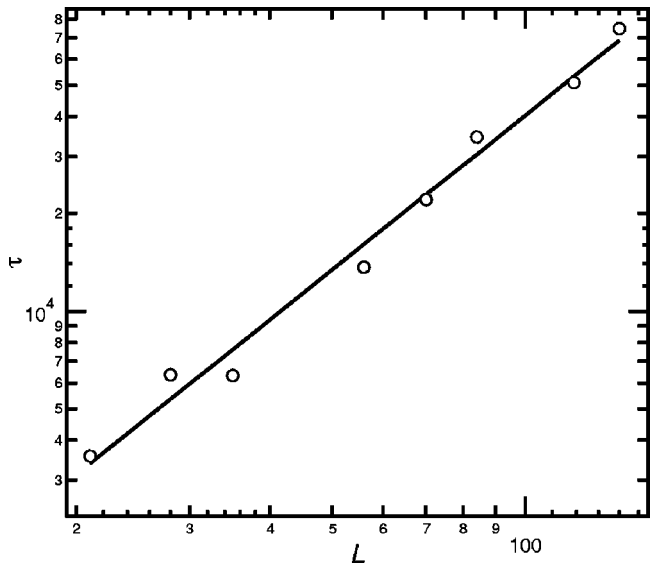

FIG. 10. Characteristic time, $\tau(L)$, as a function of the lattice size L at criticality. Simulation parameters are as in Fig. 9. The straight line has a slope of 1.59.

TABLE I. Critical exponents for the system studied in $d=2$ (present work, PW), compared with directed percolation (DP) and coupled nondiffusive conserved field (NDCF) classes in $d=2$ and $d=3$. Numbers in parentheses indicate uncertainty in the last digit.

	PW	DP[a]	NDCF[b]	NDCF[c]
d	2	2	2	3
α	1.1(1)	0.451	0.43(1)	1.3[d]
β	0.82(2)	0.584(4)	0.637(9)	0.84(2)
δ	0.82(8)	0.451(1)	0.49	0.76(3)
β'	0.62[e]	0.584(4)	0.583	0.85[e]
η	0.18(5)	0.230(1)	0.29(1)	0.16(2)
γ	$-0.64(2)$	1.60	0.84(23)	0.18(6)
$\nu_\parallel$	0.75(5)	1.295(6)	1.2(1)	1.12(8)
$\nu_\perp$	0.47[f]	0.734(4)	0.83(3)	0.62(3)
z	1.60(2)	1.76(3)	1.52(6)	1.80(5)

[a]From Ref. [25].
[b]From Refs. [35–37].
[c]From Refs. [35] and [37].
[d]Deduced from $\alpha=\beta/\nu_\parallel$.
[e]Deduced from $\beta'=\delta\nu_\parallel$.
[f]Deduced from $\nu_\perp=\nu_\parallel/z$.

(organs, tissues, cells, or enzymes). Fixing all other parameters, the system displays a nonequilibrium continuous phase transition from an active to an absorbing state as the activation probability is varied. One of the main assumptions of the model is that it does not consider spontaneous structure activation, i.e., the activation probability of a given structure in the absence of activator is zero. This could be an unrealistic approximation for product-activated allosteric enzyme networks [21], where the product usually increases the transition probability to the active state from a nonzero spontaneous probability in the absence of product. Indeed, in the presence of spontaneous activation, mean-field study shows that the absorbing-phase transition occurs for a negative value of the activation probability ω. Thus, our model can only describe self-activated networks where spontaneous activation does not occur. This is, for example, realistic in the case of cell communications via diffusive molecules, such as the growth factors auto-paracrine system, because the cell response to the activating molecule go through intracellular signal transmission pathways that do not activate in the absence of ligand-receptor complexes [6]. This seems also a reasonable assumption in the case of virus spreading, where a healthy individual cannot be infected in the absence of contact with the infectious agent. We note, however, that our model implies in this case that an infected individual eventually recovers with probability$=1$ after an infection event. Thus, our model neglects individuals removing upon infection, and is to be considered as a susceptible-infected-susceptible model as far as epidemics spreading is concerned [29]. This appears a reasonable choice for influenza spreading, because this infection is not lethal for nonimmunodepressed individuals.

We summarize in Table I the estimated values of the critical exponents, as well as their values in other models, shown for comparison. Directed percolation (DP) is the best-known universality class of second-order phase transitions to a unique absorbing state. It has proven to be very robust with respect to the microscopic dynamic rules and is thus the universality class of a wide range of models, including many reaction-diffusion ones (for a review, see Ref. [25]). One of the hallmarks of DP is a time-reversal symmetry that yields $\delta=\alpha$ (or, equivalently $\beta=\beta'$). It can be seen from Table I that this relation fails in the model studied in the present paper. Other scaling relations relate critical exponents together. For instance, DP exponents verify $\gamma=d\nu_\perp+\nu_\parallel-2\beta$ and $\eta+\delta+\alpha=d/z$ [31]. These relations are not fulfilled for the model studied in this paper. Furthermore, as can be seen from Table I, the values of most of the individual exponents disagree with two-dimensional DP. Taken toghether, these remarks strongly suggest that DP is not the universality class of the present model.

Besides DP, other absorbing-phase-transition classes have been identified in the last decade [32]. They usually emerge as a result of additional properties, such as symmetric or infinitely many absorbing states [33], particle diffusion [34], or parity conservation in the number of particles [27,28]. To our knowledge, the model which is most closely related to the present work is the reaction-diffusion model of Ref. [35]. It describes the reaction between two bosonic particles, one of which being immobile. Varying the total particle density, represented as a nondiffusive conserved field (NDCF), it exhibits an absorbing-phase transition, and is believed to define a separate universality class, to which some conserved lattice gas models also belong [36,37]. A major difference with the present work is that, in the NDCF model, the total particle density is conserved. Conservation properties are usually very important for the universality classes of absorbing-phase transitions, as exemplified by the branching-annihilating random walk models [27,28]. Surprisingly, whereas the exponents for the present model are unambiguously different from the two-dimensional NDCF class (Table I), they are close to those of the three-dimensional (3D) NDCF model. Major discrepancies are nevertheless observed, especially concerning γ, $\nu_\parallel$, and β', so that the similarity with the $3D$ NDCF class could be accidental. Finally, one of the most intriguing features of this model is the negative value for γ. This is, to our knowledge, the first observation of a negative value for this exponent, further sustaining the hypothesis of a separate universality class. Note, however, that negative values have already been reported for other exponents. For instance, in a model for quasispecies dynamics of RNA replication, field theoretical arguments have recently evidenced a negative value for η [3].

To conclude, the present model could not be unambiguously categorized in a previously described absorbing-phase-transition universality class. On one hand, this could originate from the large uncertainty in the estimates of the critical exponents. On the other hand, however, the data seems to plead in favor of a distinct set of critical exponents, which would imply a new universality class. Alternatively, in the case of the contact process for epidemics spreading, the values of the the critical exponents change continuously as the distance range of the epidemic process is continuously varied from long range to short range [38]. In the present model,

this range is mainly imposed by the product life time, indicating that the exponent values could depend on λ. To ascertain these hypotheses will need further and more intensive simulations. Studies of the one-dimensional version of the model, although of poor biological relevance, would permit more precise estimations, as well as easier comparisons with other classes.

ACKNOWLEDGMENTS

I thank Dr. Stéphane Genet, Université Paris-6, Jussieu, France, for fruitful discussions about this work. I am also indebted to Professor H. T. Diep, Laboratoire de Physique Théorique et Modélisation, Université de Cergy-Pontoise, France, for a critical reading of the manuscript.

[1] E.V. Albano, J. Phys. A **27**, L881 (1994).
[2] A. Lipowski, Phys. Rev. E **62**, 3356 (2000); M. Droz and A. Pekalski, *ibid.* **65**, 051911 (2002); C.P. Ferreira and J.F. Fontanari, *ibid.* **65**, 021902 (2002).
[3] R. Pastor-Satorras and R.V. Solé, Phys. Rev. E **64**, 051909 (2001).
[4] A. Lipowski and D. Lipowska, Physica A **276**, 456 (2000); A.F. Rozenfeld and E.V. Albano, Phys. Rev. E **63**, 061907 (2001); G. Szabó and T. Czárán, *ibid.* **63**, 061904 (2001).
[5] N.R.S. Ortega, C.F. de S. Pinheiro, T. Tomé, and J.R. Drugowich de Felício, Physica A **255**, 189 (1998).
[6] H.S. Wiley, S.Y. Shvartsman, and D. Lauffenburger, Trends Cell Biol. **13**, 43 (2003); S.Y. Shvartsman, H.S. Wiley, W.M. Deen, and D. Lauffenburger, Biophys. J. **81**, 1854 (2001).
[7] S.M. Jones and A. Kazlauskas, FEBS Lett. **490**, 110 (2001); R.K. Assoian, J. Cell Biol. **136**, 1 (1997).
[8] J.E. Kudlow and J.D. Bjorge, Semin Cancer Biol. **1**, 293 (1990).
[9] E. Ravasz, A.L. Somera, D.A. Mongru, Z.N. Oltvai, and A.L. Barabasi, Science **297**, 1551 (2002); S. Maslov and K. Sneppen, *ibid.* **296**, 910 (2002); S. Bilke and C. Peterson, Phys. Rev. E **64**, 036106 (2001).
[10] H. Levine, I. Aranson, L. Tsimring, and T.V. Truong, Proc. Natl. Acad. Sci. U.S.A. **93**, 6382 (1996).
[11] P.N. Devreotes, Neuron **12**, 235 (1994).
[12] J.H. Sorensen, D.K. Mackay, C.O. Jensen, and A.I. Donaldson, Epidemiol. Infect. **124**, 577 (2000); J. Gloster, R.F. Sellers, and A.I. Donaldson, Vet. Rec **110**, 47 (1982).
[13] S.F. Regan and C. Fowler, J. Gerontol. Nurs. **28**, 30 (2002); G.W. Hammond, R.L. Raddatz, and D.E. Gelskey, Rev. Infect. Dis. **11**, 494 (1989).
[14] A. Goldbeter and J.L. Martiel, FEBS Lett. **191**, 149 (1985).
[15] J.M. Ekboir, *Potential Impact of Foot-and-Mouth Disease in California* (University of California, Agriculture Issues Center, Davis, 1999).
[16] A.R. Kimmel and R.A. Firtel, Curr. Opin. Genet. Dev. **1**, 383 (1991).
[17] S. Miyake, M.L. Lupher, Jr., B. Druker, and H. Band, Proc. Natl. Acad. Sci. U.S.A. **95**, 7927 (1998).
[18] R.A. Vaughan and P.N. Devreotes, J. Biol. Chem. **63**, 14 538 (1988).
[19] P. Bak, C. Tang, and K. Wiesenfeld, Phys. Rev. Lett. **59**, 381 (1987); T. Hwa and M. Kardar, *ibid.* **62**, 1813 (1989); Z. Olami, H.J.S. Feder, and K. Christensen, *ibid.* **68**, 1244 (1992); P. Bak and K. Sneppen, *ibid.* **71**, 4083 (1993).
[20] J.E.S. Socolar, G. Grinstein, and C. Jayaprakash, Phys. Rev. E **47**, 2366 (1993); L. Gil and D. Sornette, Phys. Rev. Lett. **76**, 3991 (1996).
[21] A. Mikhailov and B. Hess, J. Phys. Chem. **100**, 19 059 (1996).
[22] L. Stevens, Cell **95**, 291 (1998).
[23] E.J. Doedel, Congr. Numer. **30**, 265 (1981).
[24] P. L'Ecuyer and S. Cote, ACM Trans. Math Softw. **17**, 98 (1991).
[25] H. Hinrichsen, Adv. Phys. **7**, 815 (2000); G. Ódor, e-print cond-mat/0205644.
[26] P. Grassberger, J. Phys. A **22**, 3673 (1989).
[27] I. Jensen, Phys. Rev. E **50**, 3623 (1994).
[28] D. Zhong and D. ben-Avraham, Phys. Lett. A **209**, 333 (1995).
[29] R. Pastor-Satorras and A. Vespignani, Phys. Rev. E **63**, 066117 (2001); J.D. Murray, *Mathematical Biology* (Springer Verlag, Berlin, 1993).
[30] T. Aukrust, D.A. Browne, and I. Webman, Phys. Rev. A **41**, 5294 (1990).
[31] M.A. Muñoz, R. Dickman, A. Vespignani, and S. Zapperi, Phys. Rev. E **59**, 6175 (1999).
[32] G. Ódor and N. Menyhárd, Physica D **168-169**, 305 (2002).
[33] WM. Hwang, S. Kwon, H. Park, and H. Park, Phys. Rev. E **57**, 6438 (1998); J. Hooyberghs, E. Carlon, and C. Vanderzande, *ibid.* **64**, 036124 (2001).
[34] H. Hinrichsen, Phys. Rev. E **63**, 036102 (2001); K. Park, H. Hinrichsen, and I.-M. Kim, *ibid.* **63**, 065103 (2001).
[35] R. Pastor-Satorras and A. Vespignani, Phys. Rev. E **62**, R5875 (2000).
[36] M. Rossi, R. Pastor-Satorras, and A. Vespignani, Phys. Rev. Lett. **85**, 1803 (2000).
[37] S. Lübeck, Phys. Rev. E **64**, 016123 (2001).
[38] H.K. Janssen, K. Oerding, F. van Wijland, and H.J. Hilhorst, Eur. Phys. J. B **7**, 137 (1999).